chemengineering

MDPI

Article

Thermal Decomposition Kinetic Study of Non-Recyclable Paper and Plastic Waste by Thermogravimetric Analysis

Ahmad Mohamed S. H. Al-Moftah *, Richard Marsh and Julian Steer

Cardiff School of Engineering, Cardiff University, Queen's Buildings, The Parade, Cardiff CF24 3AA, UK; marshr@cardiff.ac.uk (R.M.); steerj1@cardiff.ac.uk (J.S.)

* Correspondence: al-moftaha@cardiff.ac.uk

Abstract: The global net emissions of the Kyoto Protocol greenhouse gases (GHG), such as carbon dioxide (CO_2), fluorinated gases, methane (CH_4), and nitrous oxide (N_2O), remain substantially high, despite concerted efforts to reduce them. Thermal treatment of solid waste contributes at least 2.8–4% of the GHG in part due to increased generation of municipal solid waste (MSW) and inefficient treatment processes, such as incineration and landfill. Thermal treatment processes, such as gasification and pyrolysis, are valuable ways to convert solid materials, such as wastes into syngas, liquids, and chars, for power generation, fuels, or for the bioremediation of soils. Subcoal™ is a commercial product based on paper and plastics from the source segregated waste that is not readily recyclable and that would otherwise potentially find its way in to landfills. This paper looks at the kinetic parameters associated with this product in pyrolysis, gasification, and combustion conditions for consideration as a fuel for power generation or as a reductant in the blast furnace ironmaking process. Thermogravimetric Analysis (TGA) in Nitrogen (N_2), CO_2, and in air, was used to measure and compare the reaction kinetics. The activation energy (E_a) and pre-exponential factor A were measured at different heating rates using non-isothermal Ozawa Flynn Wall and (OFW) and Kissinger-Akahira-Sonuse (KAS) model-free techniques. The TGA curves showed that the thermal degradation of Subcoal™ comprises three main processes: dehydration, devolatilization, and char and ash formation. In addition, the heating rate drifts the devolatilization temperature to a higher value. Likewise, the derivative thermogravimetry (DTG) results stated that T_m degradation increased as the heating rate increased. Substantial variance in E_a was noted between the four stages of thermal decomposition of Subcoal™ on both methods. The E_a for gasification reached 200.2 ± 33.6 kJ/mol by OFW and 179.0 ± 31.9 kJ/mol by KAS. Pyrolysis registered E_a values of 161.7 ± 24.7 kJ/mol by OFW and 142.6 ± 23.5 kJ/mol by KAS. Combustion returned the lowest E_a values for both OFW (76.74 ± 15.4 kJ/mol) and KAS (71.0 ± 4.4 kJ/mol). The low E_a values in combustion indicate shorter reaction time for Subcoal™ degradation compared to gasification and pyrolysis. Generally, TGA kinetics analysis using KAS and OFW methods show good consistency in evaluating Arrhenius constants.

Keywords: thermal decomposition kinetic study; Subcoal™; non-isothermal; DTG; arrhenius parameters; thermogravimetric analysis; qatar national vision 2030

check for updates

Citation: Al-Moftah, A.M.S.H.; Marsh, R.; Steer, J. Thermal Decomposition Kinetic Study of Non-Recyclable Paper and Plastic Waste by Thermogravimetric Analysis. *ChemEngineering* **2021**, *5*, 54. https://doi.org/10.3390/chemengineering5030054

Academic Editor: Alírio E. Rodrigues

Received: 11 July 2021
Accepted: 20 August 2021
Published: 30 August 2021

Publisher's Note: MDPI stays neutral with regard to jurisdictional claims in published maps and institutional affiliations.

Copyright: © 2021 by the authors. Licensee MDPI, Basel, Switzerland. This article is an open access article distributed under the terms and conditions of the Creative Commons Attribution (CC BY) license (https://creativecommons.org/licenses/by/4.0/).

1. Introduction

Greenhouse effects play a valuable role in trapping heat in the atmosphere to keep the earth warm. Excessive release of GHG, such as CO_2, CH_4, and N_2O, due to increased commercial activities is invariably attributed to global warming and related climatic changes [1]. Global commitments to reduce GHG emissions and related temperature levels to pre-industrialised levels remain futile due to the slow enactment of necessary policies to reach net-zero emissions. In spite of 1260 Climate Acts across the globe and commitment by at least 20 countries to achieve net-zero emission in the next few decades, GHG emissions have maintained upward mobility [2]. The exponential demand for energy from

8588.9 million tonnes (Mtoe) to 13,147.3 Mtoe between 1995 and 2015 presents a microcosm of the future challenges posed to the Kyoto Protocol and the Paris Agreement to reduce GHG emissions to near net-zero from the current highs of 50 billion metric tonnes [3]. The composition of the GHG emissions vary considerably across the hierarchy of energy sources with fossil fuel contributing the lion share of 80%. Waste-to-energy and solid waste management practices account for 2.8–4% of the global environmental burden [4,5].

There is an increasing need to get the best use of solid wastes or biomass in thermal decomposition processes, such as pyrolysis, gasification, and combustion [6]. These processes can be utilised to decrease the reliance on fossil fuels and GHG emissions [7–9]. In a country, such as Qatar, the main practice of MSW management is landfilling, nevertheless owing to limited land availability, and this solution is increasingly not practical. Every year Qatar generates about 2.5 million tons of MSW corresponding to 1.5 kg per person per day [10]. Therefore, recycling of MSW to consumable materials and recovering energy are the more favourable options [11,12].

Subcoal™ is made from paper and plastics which are leftover from source segregated recycling waste that is deemed 'non-recyclable' after passing through municipal refuse processing facilities. The product has been considered as a high grade of solid recovered fuel (SRF), which can be converted into syngas and liquid fuels through the gasification process [13]. Alternatively, the high carbon and hydrogen content in Subcoal™ means that it is potentially suitable for consideration as an alternative reductant for ironmaking in a blast furnace, where it could either be injected directly, after milling, through tuyeres, or pre-gasified and fed directly into the furnace that way.

The understanding of pyrolysis, gasification or combustion kinetics of Subcoal™ is important for chemical reactions and mechanical designs of gasifier reactors [14,15]. In this work, the kinetic parameters were evaluated in non-isothermal TGA under N_2, CO_2, and air atmosphere using Ozawa Flynn Wall (OFW) and the Kissinger-Akahira-Sonuse (KAS) model-free approaches. In addition, this is the first research paper studying the thermal and kinetic behaviours of Subcoal™ PAF using TGA. The thermal degradation (DTG) was carried out, and the conversion degree of Subcoal™ PAF was determined as a function of temperature. The E_a of Subcoal™ PAF were compared with other similar solid waste and biomass examples from the literature.

2. Materials and Methods

2.1. Materials

Subcoal™ has been supplied by the international N+P Group B.V. (Bergen, The Netherlands). It is usually supplied in the form of pellets, but, for the purposes of this study, the Pulverised Alternative Fuel (PAF) has been used as a milled product as a powder <3 mm particle size. The outcomes of the proximate and ultimate analysis of Subcoal™ are listed in Table 1.

Table 1. Proximate and ultimate analysis of Subcoal™.

Proximate Analysis (wt, %)		Ultimate Analysis (wt, %)	
Moisture content	3.1 ± 0.4	C	45.7 ± 2.7
Ash	11.8 ± 0.5	H	6.4 ± 0.2
Volatile matter content	77.6 ± 1.4	S	0.2 ± 0.06
Fixed carbon	7.5 ± 1.4	N	0.6 ± 0.2
Gross calorific value, (MJ/kg)	23.1 ± 2.8	O (by difference)	35.3 ± 1.9
Density, kg/m^3	450		

Thermogravimetry (TG) and the DTG was performed in a Mettler Toledo analyser (TGA/SDTA 851e) between temperature range of 25 °C to 900 °C. The effect of heating rates on the thermal decomposition process was examined and compared with the literature by adopting four heating rates: 5, 10, 15, and 20 °C/min. A crucible was made of alumina. To make sure the sample is well distributed, the crucible was gently tapped on a solid surface. Pyrolysis was performed under a N_2 flow rate of 50 mL/min, while gasification

was performed under CO_2 flow rate of 100 mL/min and combustion was performed under air flow rate of 100 mL/min atmosphere. The flow rate setting for different gases was chosen based on the optimum operating condition of the TGA instrument and to compare the result with the literature.

Sample weight loss was continuously recorded against the temperature to obtain the TGA curve that was derived later for the first-order derivative to get the DTG curve. All experiments were repeated three times to eliminate experimental errors and to check the reproducibility of all experiments.

2.2. The Measurement of the Kinetic Parameters of the Reaction

The reaction kinetics depend on reactant concentrations, temperature, pressure, and the presence of catalysts. Among reaction kinetics components, rate of reaction (r), which describes the reaction speed, is expressed as follows:

$$r \propto [B]^n, \tag{1}$$

where $[B]$ is a reactant concentration, and n the reaction overall order. The rate of reaction is proportional to the reaction constant (k):

$$r = k[B]^n, \tag{2}$$

$$\frac{d[A]}{dt} = k[B]^n. \tag{3}$$

The response of reaction to the change in these factors is determined by the reaction constant (k). The value of k changes with temperature based on the mathematical correlation initially proposed by Arrhenius [16]:

$$k = A\, e^{\frac{-E_a}{RT}}. \tag{4}$$

Both (E_a) and (A) are known as kinetic constants and independent on temperature. As the measurement of reactant concentration is unachievable during the process, reactant concentration [B] can be expressed as a function of fractional conversion (x). Therefore, the rate of reaction in Equation (3) can be given in the following expression:

$$\frac{dx}{dt} = k(T)f(x). \tag{5}$$

The $f(x)$ represents the overall gasification reaction model. By combining Equations (4) and (5), the following equation is obtained:

$$\frac{dx}{dt} = \left[A\, e^{\frac{-E_a}{RT}}\right] f(x). \tag{6}$$

The sample mass loss from the analysis is used to calculate the conversion (x) based on the following formula:

$$x = \frac{m_o - m_t}{m_o - m_f}. \tag{7}$$

The initial sample mass is given by m_o, the measured mass m_o as it changes, and m_f, the final mass after complete conversion. Therefore, data of conversion degree, heating rate and temperature are then used by a kinetic analysis method to determine the kinetic parameters.

2.3. Ozawa–Flynn–Wall (OFW) Method

The OFW method is an iso-conversational and integral model free method that includes measurement of the temperature at given values of conversion at various heating

rates [17]. In this method, Equation (9) is integrated utilizing Doyle's approximation to evaluate the kinetic constants.

$$ln(\beta) = ln\left(\frac{A\ E_a}{R\ g(x)}\right) - 4.9575 - 1.052\frac{E_a}{RT}. \quad (8)$$

The E_a can be obtained from the slope by plotting term $ln(\beta)$ against $\frac{1}{T}$, where the term $\ln\left(\frac{A\ E_a}{R\ g(x)}\right) - 4.9575$ is the integration constant that can be determined from the y-intercept. The following relationship can be used to determine A for known values of x and E_a:

$$A = \frac{-\beta\ R}{E_a}\ (ln[1-x])\ 10^a, \quad (9)$$

where a is a numerical integration constant based on the Doyle approximation.

2.4. Kissinger-Akahira-Sunose (KAS)

KAS is an alternative model free method that considers in the derivation the peak temperature (T_m) at the maximum reaction rate value. Therefore, this method adopts the following equation to estimate the E_a for different values of T_m and β.

$$ln\frac{\beta}{T_m^2} = ln\left(\frac{R\ A}{g(x)\ E_a}\right) - \frac{E_a}{R\ T}. \quad (10)$$

For a progressive value of conversion degree, the term $\ln\frac{\beta}{T_m^2}$ is plotted against $\frac{1}{T}$ to give a straight-line slope of $\frac{E_a}{R}$; hence, the apparent E_a can be determined, while the value of A can be calculated from Equation (11).

$$A\ (\beta) = \frac{\beta\ E_a}{R\ T_m^2}\ e^{-\frac{E_a}{R\ T_P}}. \quad (11)$$

3. Result and Discussion

3.1. Thermal Parameters

Figures 1–3 display the reaction conversion (X) in (a) and show DTG weight loss (wt %/min) profile in (b) for different heating rates in N_2, CO_2, and air, respectively. The conversion is estimated as a reciprocal of the fractional mass loss. The higher the rate of conversion, the faster the thermal decomposition or rate of reaction. Tables 2–4 show thermal decomposition parameters of Subcoal™ PAF in N_2, CO_2, and air atmosphere. The results show that most of the sample material was converted to products in the temperature range of 250 °C to 550 °C as confirmed by Slopiecka et al., in 2012 [18]. The raising of heating rate shifts the curve of fractional extent conversion to a high temperature region. The heating rate increases the initial temperature of decomposition (Onset temperature) [19].

Table 2. Thermal decomposition of Subcoal™ PAF in N_2 from TGA curves.

	First Stage			Second Stage			Third Stage			Fourth Stage		
β °C/min	Start * (°C)	End ** (°C)	Weight Loss (%)	Start * (°C)	End ** (°C)	Weight Loss (%)	Start * (°C)	End ** (°C)	Weight Loss (%)	Start * (°C)	End ** (°C)	Weight Loss (%)
5	28.2	156.9	3.6	233.5	376.3	34.2	376.3	471.4	41.4	636.6	688.1	11.2
10	28.8	156.5	4.7	233.5	378.6	35.6	378.6	493.8	42.6	638.6	693.7	11.4
15	28.1	157.3	4.9	233.5	395.6	37.6	395.6	510.4	45.7	640.5	712.4	9.2
20	27.7	158.9	5.2	233.5	426.7	39.6	426.7	522.2	48.5	641.6	732.4	4.7
Average	28.2	157.4	4.6	233.5	394.3	36.8	394.3	499.5	44.3	639.3	706.7	9.1

* Start refers to start (onset) temperature of an indicated decomposition step. ** End refers to end (offset) temperature of an indicated decomposition step.

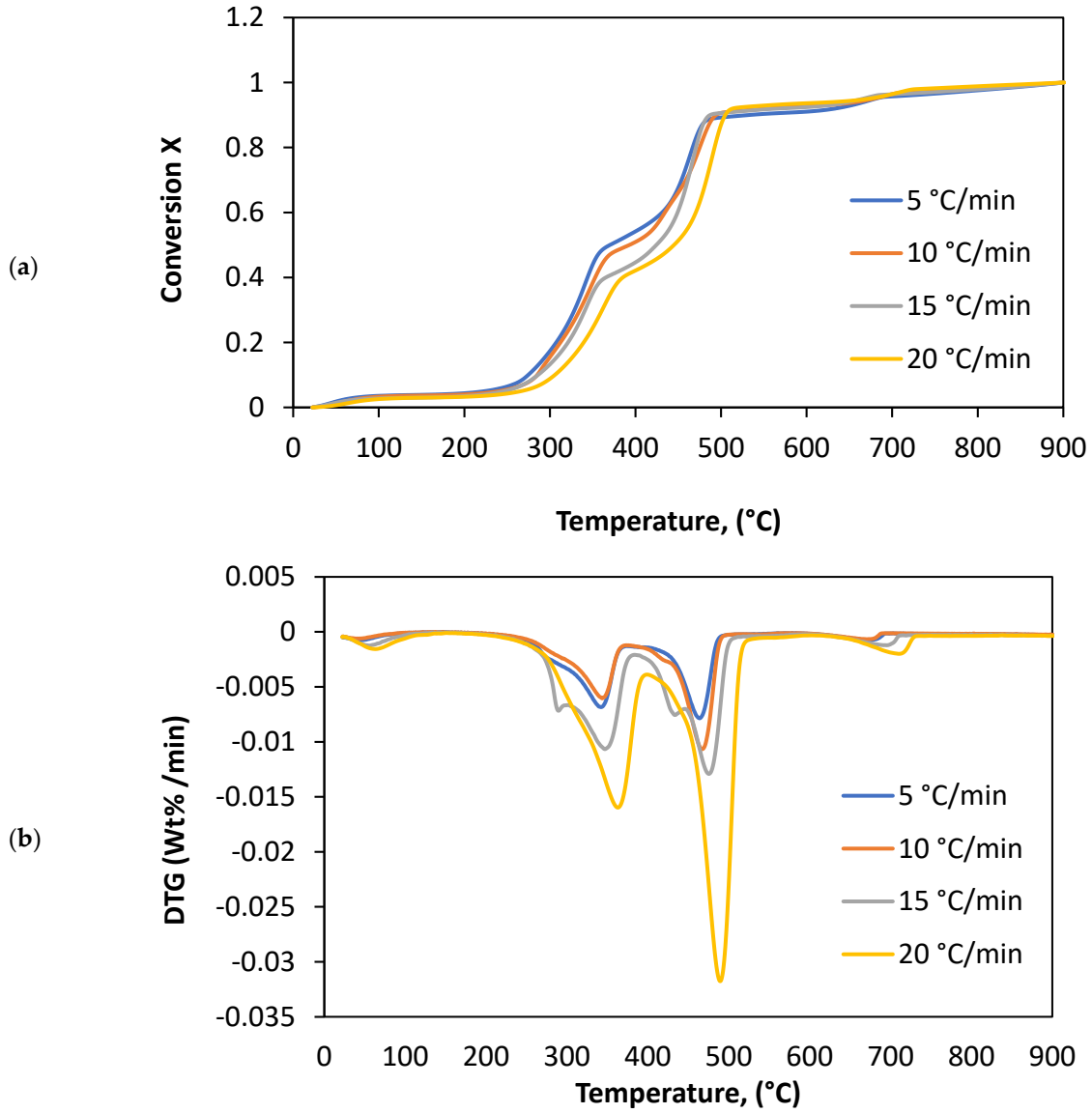

Figure 1. The effect of the heating rate in N_2: (**a**) conversion degree and (**b**) DTG weight loss.

Table 3. Thermal decomposition of Subcoal™ PAF in CO_2 from TGA curves.

	First Stage			Second Stage			Third Stage			Fourth Stage		
β °C/min	Start * (°C)	End ** (°C)	Weight Loss (%)	Start * (°C)	End ** (°C)	Weight Loss (%)	Start * (°C)	End ** (°C)	Weight Loss (%)	Start * (°C)	End ** (°C)	Weight Loss (%)
5	28.6	167.6	3.4	199.2	380.4	34.2	380.4	483.4	51.2	622.2	658.3	3.8
10	28.5	166.2	3.6	199.2	410.3	34.6	410.3	489.6	50	622.2	692.2	3.9
15	28.4	164.4	3.8	199.2	412.2	37.3	412.2	550.6	41.6	622.2	708.9	4.4
20	28.7	163.8	3.9	198.3	428.6	38.5	428.6	558.4	42.3	623.4	792.7	5.5
Average	28.6	165.5	3.7	198.9	407.9	36.2	407.9	520.5	46.3	622.5	713.0	4.4

* Start refers to start (onset) temperature of an indicated decomposition step. ** End refers to end (offset) temperature of an indicated decomposition step.

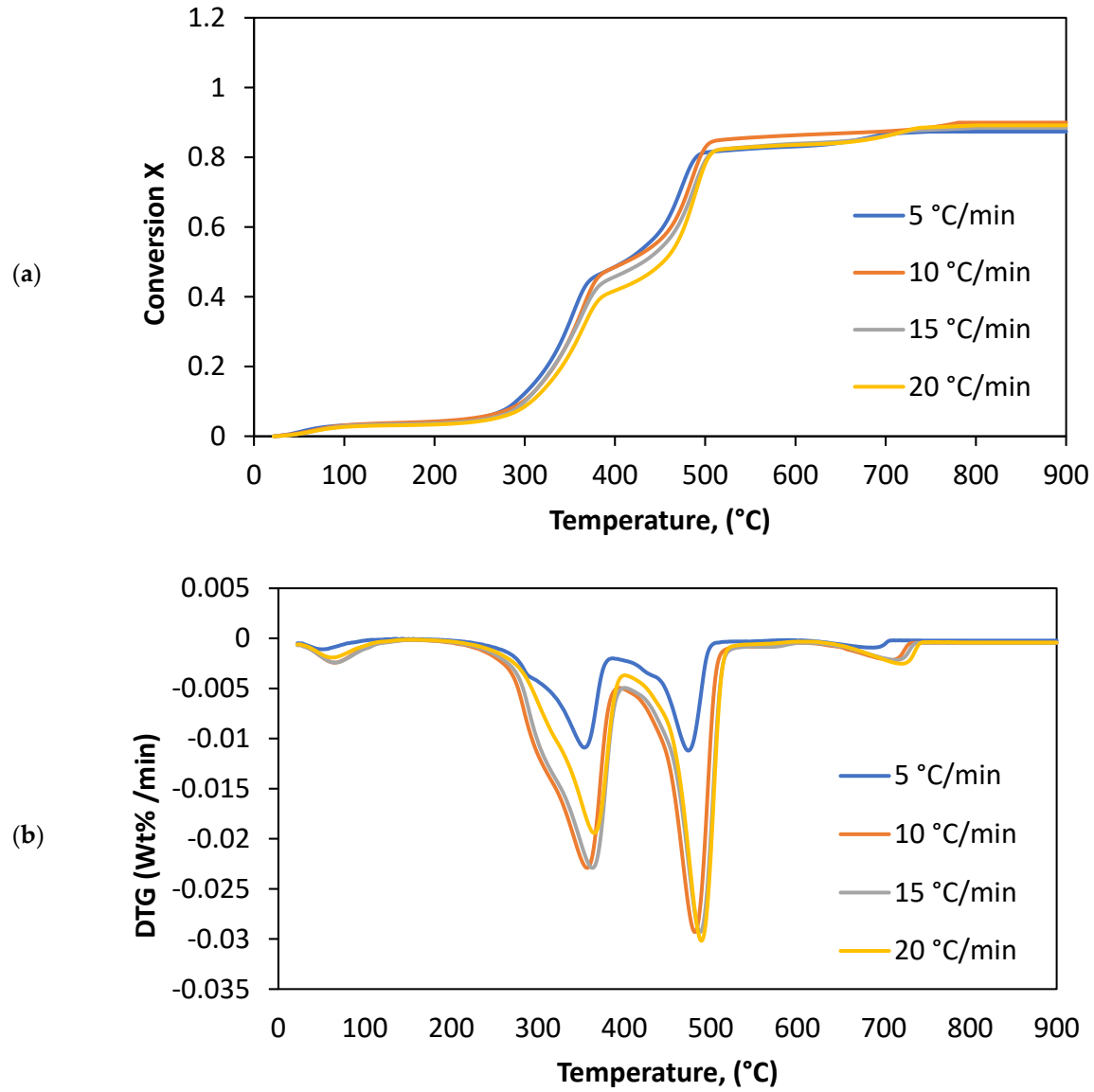

Figure 2. The effect of the heating rate in CO_2: (**a**) conversion degree and (**b**) DTG weight loss.

Table 4. Thermal decomposition of Subcoal™ PAF in air from TGA curves.

	First Stage			Second Stage			Third Stage			Fourth Stage		
B °C/min	Start * (°C)	End ** (°C)	Weight Loss (%)	Start * (°C)	End ** (°C)	Weight Loss (%)	Start * (°C)	End ** (°C)	Weight Loss (%)	Start * (°C)	End ** (°C)	Weight Loss (%)
5	28.4	140.3	4.3	214.2	332.5	33.4	332.5	478.6	52.7	615.5	655.3	3.2
10	28.2	150.4	4.6	214.2	347.5	34.3	347.5	524.6	52.1	615.5	690.2	3.7
15	28.6	150.2	4.4	214.3	358.3	35.3	358.3	534.5	42.3	616.3	705.9	4.5
20	28.2	160.4	5.3	214.5	385.1	38.9	385.1	546.2	42.6	617.5	745.8	5.4
Average	28.3	150.3	4.7	214.3	355.9	35.5	335.9	521	47.4	616.2	699.3	4.2

* Start refers to start (onset) temperature of an indicated decomposition step. ** End refers to end (offset) temperature of an indicated decomposition step.

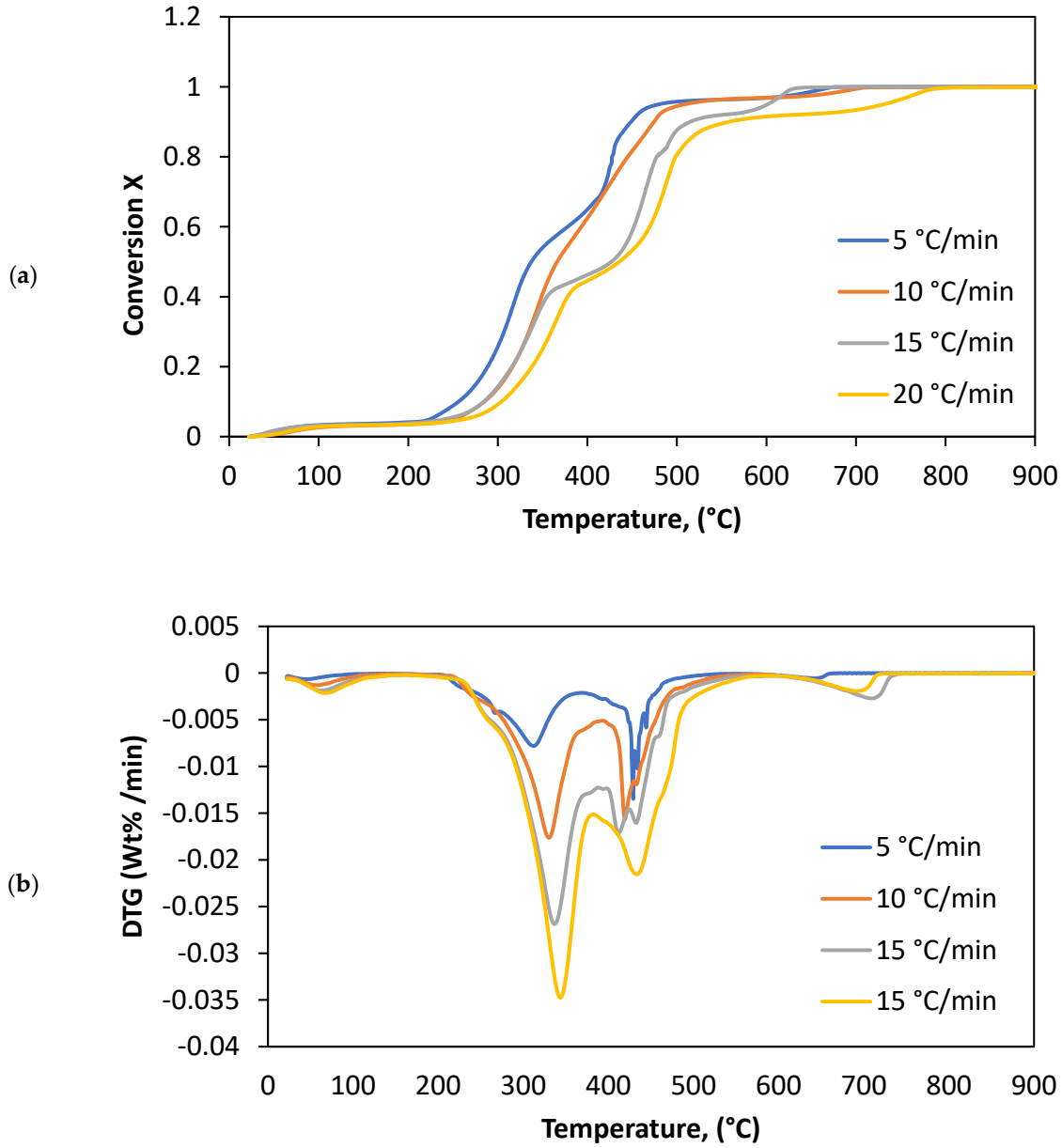

Figure 3. The effect of the heating rate in air: (**a**) conversion degree and (**b**) DTG weight loss.

As the heating rates increases, the T_m within the sample rises, which leads to faster chemical reaction kinetics and Subcoal™ PAF conversion to gaseous products [20]. Moreover, the lower the heating rate, the longer the reaction residence time, and, hence, the lower amount of Subcoal™ PAF converts.

The conversion curve represents fourth stages of sample decomposition. In the first stage, for temperature less than 150 °C, it is during the dehydration process that the volatile material and moisture leave the sample with insignificant changes in the mass. Then, in the second and third stages, a region between 250 °C to 550 °C, which is known as active conversion, the sample losses most of its mass in the devolatilization process. In the final stage, only ash and char are left, which is less than 15% of the sample mass [21]. The weight slowly reduces in the first and the last stage, which is known as the passive reaction.

According to the DTG curves for Subcoal™ PAF under N_2, CO_2, and air at various heating rates, as the heating rate increase, the peaks become clearer and larger. The initial and the final temperature of the pyrolysis, gasification, and combustion stages are drifted with increase in heating rate. The results form TG and DTG illustrate that the thermal peak position is not fixed when the heating rate changed. The endothermic peaks, which are the

decomposition reaction, are observed in the DTG curves at each tested heating rate [22]. The restriction of heat transmission from the surrounding to the test sample may explain the temperature shifting to higher values. At a high heating rate, the residence time of reaction is short, and the temperature needed to devolatilise becomes greater. However, when the process occurs at a low heating rate, the instantaneous thermal energy is high with a longer reaction time that makes the reaction temperature is lower [23]. Hence, its clearer to see that mass changes at higher heating rates.

Table 5 lists the maximum peak temperatures (T_m) at which there is the higher DTG (wt %/min). Tm increase with a heating rate increase during pyrolysis, gasification, and combustion process. The average standard deviation (±) values of peak temperature and degradation rate was calculated from the third run results.

Table 5. Thermal decomposition of Subcoal™ PAF parameters in different atmospheres.

	N_2		CO_2		Air	
β °C/min	T_m °C	DTG_{Tm} wt %/min	T_m °C	DTG_{Tm} wt %/min	T_m °C	DTG_{Tm} wt %/min
5	471 ± 7.0	−0.0094 ± 0.0014	466 ± 5	−0.0097 ± 0.0014	317 ± 4.2	−0.0071 ± 0.0009
10	481 ± 6.7	−0.019 ± 0.0057	474 ± 6	−0.019 ± 0.0079	335 ± 13.4	−0.015 ± 0.0024
15	486 ± 4.8	−0.021 ± 0.0056	482 ± 5	−0.029 ± 0.0073	336 ± 2.0	−0.025 ± 0.0027
20	487 ± 1.1	−0.032 ± 0.006	488 ± 1.2	−0.032 ± 0.002	340.3 ± 10.5	−0.016 ± 0.0082

The value of T_m increased from 471 ± 7 °C to 487.1 ± 1.1 °C, and DTG_{TM} increased from −0.0094 ± 0.0014 wt %/min to −0.032 ± 0.006 wt %/min, for pyrolysis when the heating rate raised from 5 to 20 °C/min. In addition, T_m increased from 466 ± 5 °C to 488 ± 1.2 °C, and DTG_{TM} increased from −0.0097 ± 0.0014 wt %/min to −0.032 ± 0.002 wt %/min, for gasification. However, combustion showing lowest temperature degradation results, T_m increased from 317 ± 4.2 °C to 340.3 ± 10.4 °C, and DTG_{TM} increased from −0.0071 ± 0.0009 wt %/min to −0.016 ± 0.0082 wt %/min, thus the combustion process showing faster mass loss with lower T_m value due to high oxidation reaction. The rate of Subcoal™ PAF degradation DTG and T_m increased with the heating rate, which is coherent with the literature [24].

Comparing Subcoal™ PAF results in TGA to the literature, Gerassimidou et al., in 2020, found the N_2 pyrolysis of SRF T_m = 500 °C and for paper waste T_m = 575 °C, at 20 °C/min. In addition, the pyrolysis results of paperboard show T_m = 732 °C, while the oxidation of SRF results show T_m = 600 °C. This result proves that thermal degradation of Subcoal™ pyrolysis and oxidation is lower than SRF, paper waste, and paperboard [25].

3.2. Kinetic Parameters

OFW and KAS methods were used in the present work to determine the E_a and A of three decomposition processes of Subcoal™ PAF. In OFW, the E_a was graphically estimated from the slope of Equation (9), as presented in Figure 4a–c, and A value was determined using Equation (10). Table 6 states the kinetic parameters from TGA. As observed, a significant variation is clear in the E_a as the conversion increased from 0.2 to 0.8, which indicates the multistage characteristic of the reaction mechanism. Plots of KAS method in Figure 5a–c show a high degree of linearity, hence high numerical stability of the method. The average correlation coefficient (R^2) of the three runs exceeds 0.9. The plot of E_a and A estimation was executed according to Equation (11), summarised in Table 7.

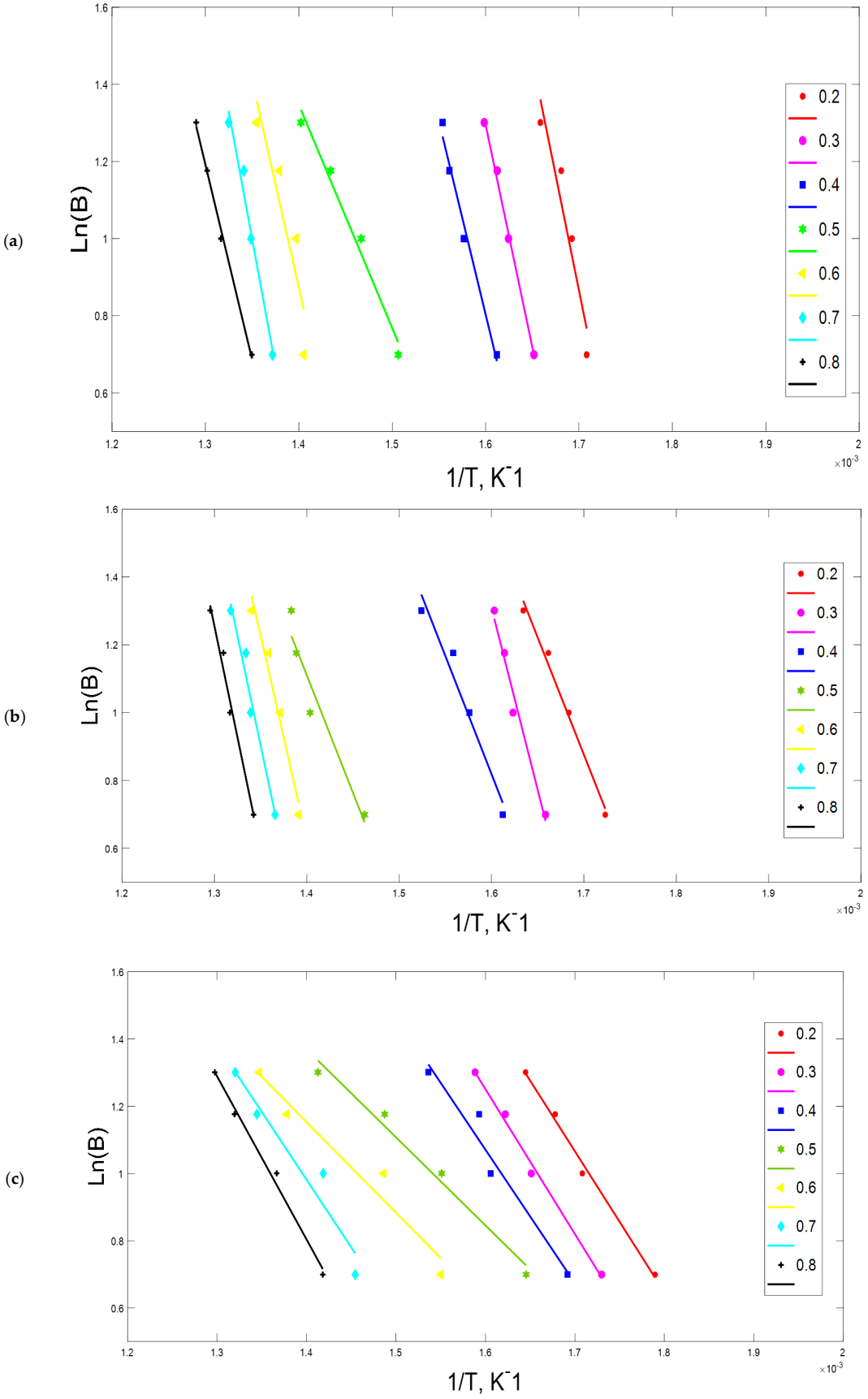

Figure 4. The approximated curves of OFW method of pyrolysis (**a**), gasification (**b**), and combustion (**c**) of Subcoal™ PAF for different values of conversion at heating rates of 5, 10, 15, and 20 °C/min.

Table 6. Kinetic parameters obtained by OFW method.

	N_2			CO_2			Air		
X /	E_a (kJ/mol)	R^2 /	A (min^{-1})	E_a (kJ/mol)	R^2 /	A (min^{-1})	E_a (kJ/mol)	R^2 /	A (min^{-1})
0.2	118.9	0.802	2.7×10^9	139.2	0.988	1.5×10^{11}	84.6	0.993	2.7×10^6
0.3	142.5	0.995	1.6×10^{11}	216.5	0.977	6.4×10^{10}	86.8	0.993	2.2×10^6
0.4	161.9	0.996	2.7×10^{13}	140.4	0.959	5.1×10^{10}	80.0	0.957	2.2×10^6
0.5	71.9	0.966	6.9×10^4	139.6	0.934	4.1×10^9	52.8	0.981	2.0×10^6
0.6	165.4	0.970	2.7×10^{11}	241.4	0.968	1.4×10^9	54.2	0.951	1.0×10^6
0.7	207.2	0.857	2.4×10^{14}	259.5	0.967	1.1×10^9	81.1	0.934	4.6×10^5
0.8	264.2	0.931	2.4×10^{18}	264.6	0.981	9.5×10^8	97.7	0.991	3.5×10^5
Average	161.7	0.931	3.4×10^{17}	200.2	0.968	4.0×10^{10}	76.7	0.971	1.6×10^6
E_a	161.7 ± 24.7			200.2 ± 33.6			76.7 ± 15.4		

(**a**)

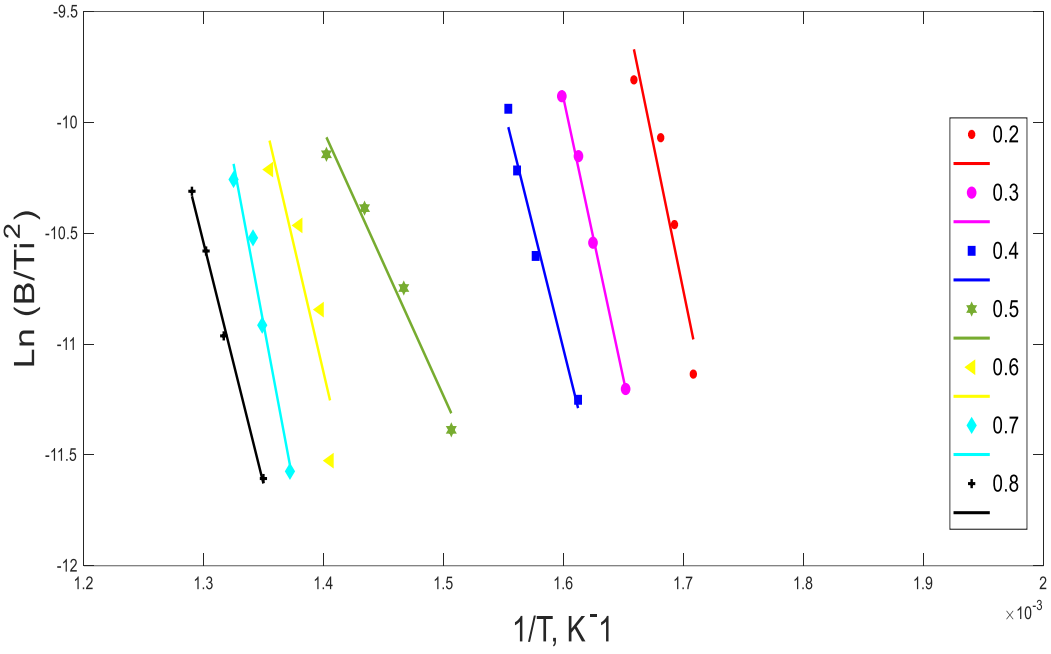

(**b**)

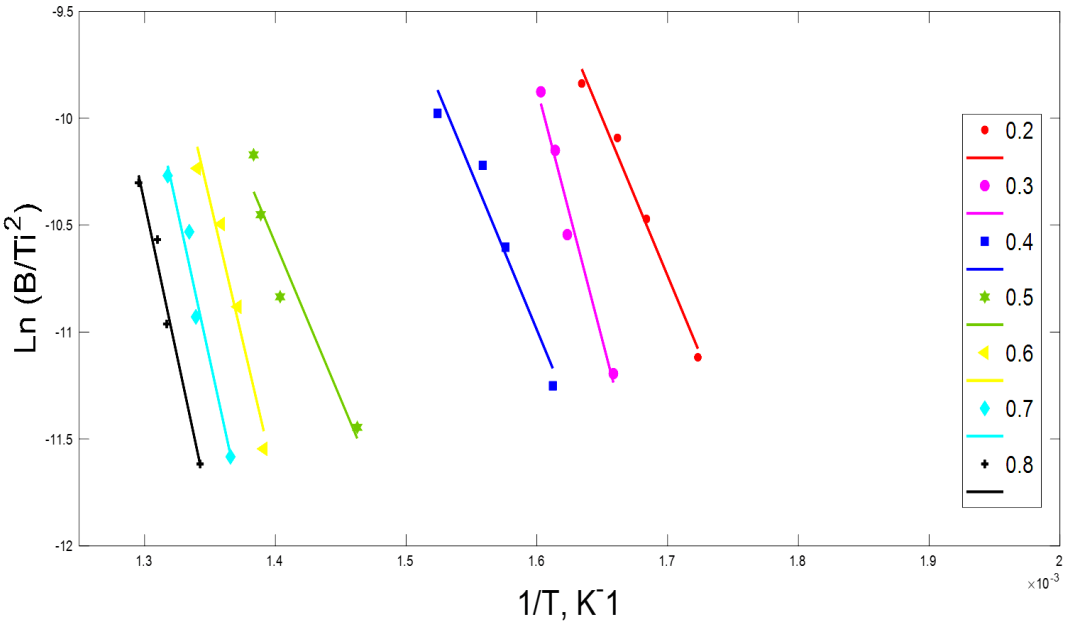

Figure 5. *Cont.*

(**c**)

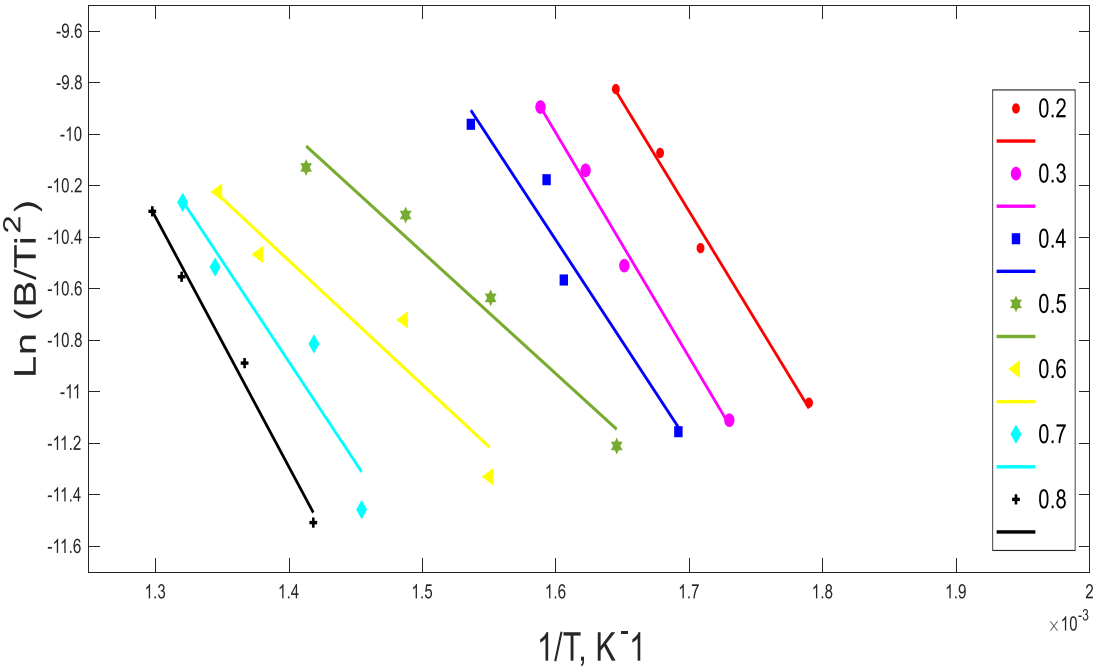

Figure 5. KAS diagrams of pyrolysis (**a**), gasification (**b**), and combustion (**c**) of Subcoal™ PAF for given values of conversion at heating rates of 5, 10, 15, and 20 °C/min.

Table 7. Kinetic parameters obtained by KAS method.

	N_2			CO_2			Air		
X **/**	E_a **(kJ/mol)**	R^2 **/**	***A*** **(min^{-1})**	E_a **(kJ/mol)**	R^2 **/**	***A*** **(min^{-1})**	E_a **(kJ/mol)**	R^2 **/**	***A*** **(min^{-1})**
0.2	103.2	0.771	1.8×10^{8}	122.5	0.986	4.8×10^{7}	46.9	0.957	9.9×10^{2}
0.3	125.3	0.994	2.0×10^{10}	195.7	0.974	1.1×10^{13}	53.6	0.958	4.3×10^{3}
0.4	143.9	0.996	9.8×10^{11}	122.9	0.952	5.2×10^{7}	59.3	0.977	1.5×10^{4}
0.5	57.1	0.951	9.4×10^{3}	121.1	0.922	3.8×10^{7}	57.6	0.918	1.1×10^{4}
0.6	145.3	0.965	1.3×10^{12}	217.4	0.964	3.9×10^{14}	62.5	0.914	3.0×10^{4}
0.7	184.7	0.840	4.9×10^{15}	234.8	0.963	6.6×10^{15}	107.9	0.856	5.0×10^{8}
0.8	238.8	0.924	3.7×10^{20}	239.5	0.979	1.4×10^{16}	109.3	0.927	6.8×10^{8}
Average	142.6	0.920	5.3×10^{19}	179.6	0.963	3.1×10^{15}	71.0	0.925	1.7×10^{8}
E_a	142.6 ± 23.5			179.0 ± 31.9			71.0 ± 4.4		

The E_a for pyrolysis obtained by OFW is 161.7 ± 24.7 kJ/mol and 142.6 ± 23.5 kJ/mol by KAS. In addition, the E_a for gasification obtained by OFW is 200.2 ± 33.6 kJ/mol and 179.0 ± 31.9 kJ/mol by KAS. However, the E_a for combustion obtained by OFW is 76.7 ± 15.4 kJ/mol and 71.0 ± 4.4 kJ/mol by KAS. Thus, combustion results show lower E_a and indicate that shorter time required for Subcoal™ PAF degradation than pyrolysis or gasification. The slight differences in average E_a might be owed to the improper approximation of temperature integration [26]. These findings are confirmed by (Guida et al., 2019).

Figure 6a,b shows OFW and KAS methods are in good relation to each other and indicate that the reaction mechanism of Subcoal™ is a complex multi-step reaction. The degradation rate from 0.2 to 0.5 shows that the E_a is almost stable, referring to the fact that one reaction one reaction mechanism is taking place in the solid phase. Then, from 0.5 to 0.8 conversion, the E_a raises and fall again by both methods.

(**a**)

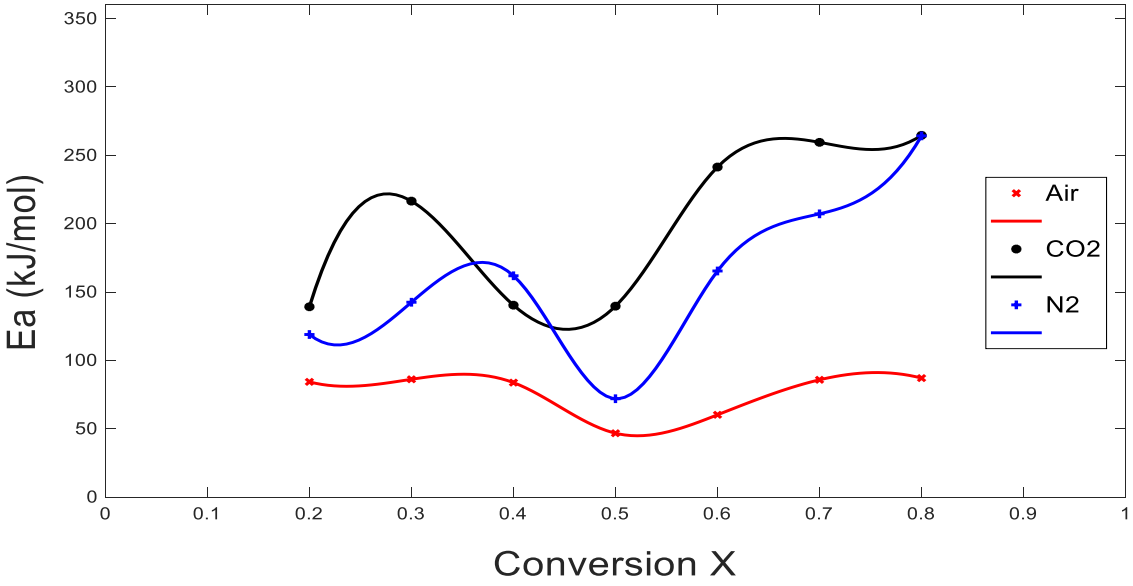

(**b**)

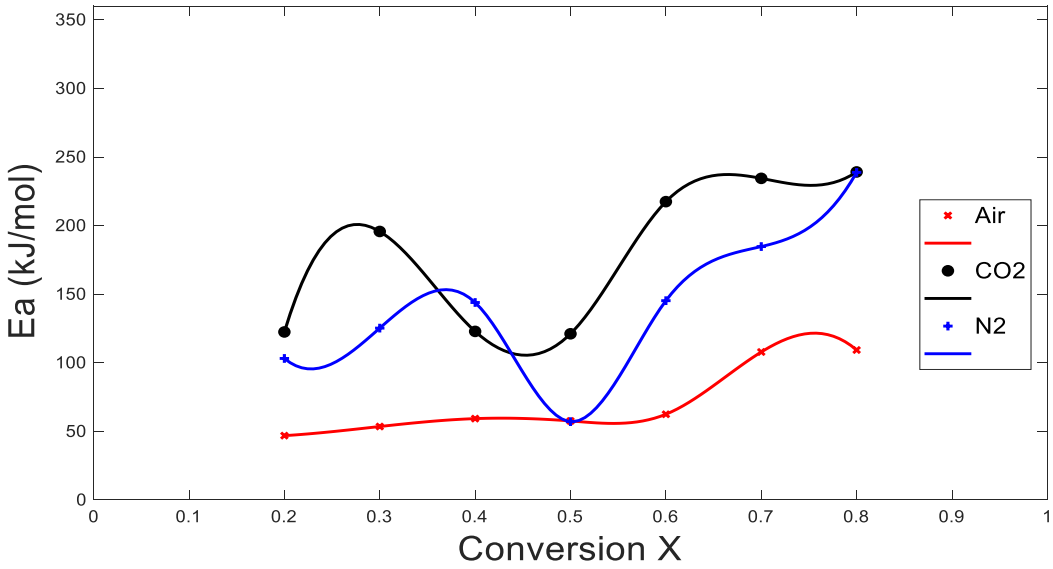

Figure 6. Compression plots of E_a as a function of conversion (X): (**a**) OFW and (**b**) KAS.

Comparing E_a of Subcoal™ results with the literature, Singh et al., in 2012, found that pyrolysis of MSW E_a 294.8 kJ/mol [27], and Chen et al., in 2015, reported that the E_a of MSW in CO_2 gasification for polyester fabrics is 211 kJ/mol, and polyethylene (PE) is 221 kJ/mol [28]. In addition, (Azam), in 2019, identified the E_a of MSW combustion as 116.1 kJ/mol [29]. However, the E_a of refuse derived fuel (RDF) and SRF combustion are 203 kJ/mol and 86.8 kJ/mol [30]. In addition, the E_a of RDF and SRF pyrolysis are 252.5 kJ/mol and 238.3 kJ/mol [31]. These results prove that the E_a of Subcoal™ PAF is lower than others biomass from the literature, resulting in an upsurge in chemical reaction, and more particles will collide, with enough energy.

4. Discussion

4.1. Thermal Analysis

Thermal behaviour of Subcoal™ PAF is described as a complex of non-recyclable paper-plastic mixture consists of four decomposition stages. Heating rate is an essential parameter in the estimation of the E_a and A using the non-isothermal TGA data. It provides

an important parameter of sample concerning decomposition temperature ranges and kinetics. In addition, at various heating rates, exposure of biomass particles (residence time) varies, which changes the thermal degradation process. An inaccurate determination of the heating rate may lead to imprecise estimation of the kinetic constants. Miscalculation of the heating rate is one of the significant sources of error in the kinetic evaluation. The assumption of the actual heating rate is the main reason for the heating rate miscalculation. Other factors may contribute to inaccurate determination of heating rate are self-heating/cooling and purge gas cooling [32]. Increasing heating rates raised the reaction rates, and it speeds up the motion of molecules, which force the reaction to collide.

The combustion reaction began earlier than pyrolysis process since pyrolysis was undertaken without air or oxygen. Instead, in combustion, a high amount of oxygen can help and accelerate the heating process. For gasification, it can be identified that, at the beginning of the process, pyrolysis occurred.

The degradation of Subcoal™ PAF in CO_2 atmosphere looks like a complex mechanism, more than N_2 and air, due to presence of high oxygen content that promotes successive oxidation reactions affecting the degradation rate [33]. However, T_m values are directly proportional to the heating rate; hence, pyrolysis needs more time to reach complete conversion [34]. In all experiments, mass loss curves at 15 °C/min and 20 °C/min are close to each other and are overlapping at some points. This may explain the complexity of Subcoal™ PAF degradation process, especially in CO_2 and air atmosphere. However, in this situation, the limitations of diffusion and heat transfer restrictions had a pronounced impact [35].

The final stage (stage IIII) is where the char and ash forms and degrades to volatile gases in the temperature range of 600 to 800 °C, with small variation in the mass loss [26]. The temperature range in the fourth stage is known as a critical temperature because of an insignificant change of mass with a continuous increase in temperature [36]. The heating rate plays a vital role in the thermal degradation process of Subcoal™ PAF in TGA. The results indicate that the increase in heating rate increases reaction rate of the decomposition process and decrease the time required to start stages. In addition, the lower the heating rate, the greater the temperature is needed to initiate the degradation. Moreover, the heating rate prolongs the period to achieve the equilibrium; therefore, it was shifted to a higher temperature region as a result of slow heat diffusion [37]. Subcoal™ PAF is decomposed in a large temperature range at lower levels than fossil fuels because of its low fixed-carbon and high volatile matter. Thus, combining Subcoal™ PAF with other biomass or fuels, such as coal, can mitigate emissions and provide some economic solutions to energy sectors.

In the DTG analysis, the degradation rate in wt %/min is plotted against the temperature. The peaks that appear in the graph show the amount of degradation that occurred at a specific temperature range. The value of T_m determines the performance of Subcoal™ PAF degradation in TGA. The results show that two small peaks are corresponding to degradation in the first and fourth stages, respectively, as well as two large peaks in the second stage [21]. T_m increases with increase in heating rate, which indicates that shorter reaction time is required to complete the reaction [22]. The peaks overlapping and the irregularity of peak shape indicate the occurrence of simultaneous reactions [26].

4.2. Kinetic Analysis

The kinetic evaluation is very important for identifying the operating conditions of thermal degradation process for Subcoal™ PAF [38]. The E_a of pyrolysis, gasification, and combustion were evaluated in TGA to identify the minimum energy required for a reaction to occur. OFW and KAS are most popular and accurate model-free techniques and were used during analysis. Linear regression results obtained from the OFW and KAS methods indicate that the E_a and A increase as the conversion increased [18]. The E_a obtained by OFW was slightly different than KAS in the average standard deviation due to the improper approximation of temperature integration, as confirmed by Guida

et al. (2019). This variation in estimation can be neglected for some applications of the OFW method, which refers to the complexity of the reaction mechanism [39]. The findings of both methods stated that the E_a is dependent on conversion. The higher complexity of dehydration process, the greater the variation of E_a [40]. Thus, Subcoal™ PAF ignition point is considerably low compared to RDF or SRF. Pyrolysis, gasification and combustion results of Subcoal™ PAF in TGA results provide lower E_a than MSW, RDF, and SRF.

As part of Qatar national vision 2030 one of the aims is to have the lowest possible CO_2 footprint, and, instead of MSW incineration or landfill, the non-recyclable paper and plastic waste can be utilised as a substitute fuel in waste-to-energy plant for sustainable power production. It is a good substitute for fossil fuels that will help generate energy sustainably [41].

In addition, Subcoal™ can be used to replace fossil fuels in cement and lime plants, steel blast furnaces, and power generation facilities. The N+P won huge contracts to supply Subcoal™ to the Uskmouth coal-fired power station in south Wales and Teesside plant in the United Kingdom because of its high conversion efficiency to renewable energy.

5. Conclusions

The kinetic parameters of biomass thermal degradation are essential for the design of the chemical reactor. This work aims to investigate the E_a and A of non-recyclable paper and plastic waste (Subcoal™ PAF) in N_2, CO_2, and air environment. The kinetic evaluation of the experimental TGA data carried out using OFW and KAS model-free methods. The experiments of thermal conversion were performed using the TGA method, whereby the sample mass loss was measured as a function of time and temperature at various heating rates. The DTG data was also obtained in terms of the degradation rate. Four peaks were obtained during degradation process may be attributed to Subcoal™ heterogeneity. From the TGA results, the Subcoal™ PAF degradation includes three process: dehydration, devolatilization, and char and ash degradation. The heating rate shifts the temperature range of the devolatilization process to higher values. The degradation of Subcoal™ in CO_2 atmosphere tends to be a complex mechanism, as shown by the DTG graphs, while combustion results obtained excellent E_a and A parameters.

The E_a of Subcoal™ PAF obtained in this work for pyrolysis, CO_2 gasification, and combustion are lower than E_a of SRF/RDF obtained in the literature. This result proves that Subcoal™ PAF provides a faster chemical reaction time than SRF/RDF and other biomass.

Subcoal™ technology improves utilisation of MSW and prevents landfill, as a result of meeting the increasing demand for lower emissions and high-calorie fuels. It is a crucial sustainable technology that helps utilisation of non-recyclable materials in energy sectors that could otherwise be lost into landfills.

Author Contributions: Conceptualization, A.M.S.H.A.-M., R.M. and J.S., investigation, A.M.S.H.A.-M.; resources, A.M.S.H.A.-M.; writing—original draft preparation, A.M.S.H.A.-M.; writing—review and editing, R.M. and J.S.; supervision, R.M., and J.S. All authors have read and agreed to the published version of the manuscript.

Funding: This work is financially supported by Qatar National Research Found, member of Qatar Foundation for Education, Science and Community Development for doctoral project number GSRA5-1-0404-18034.

Institutional Review Board Statement: Not applicable.

Informed Consent Statement: Not applicable.

Data Availability Statement: Not applicable.

Acknowledgments: The authors thank Cardiff University for its technical support.

Conflicts of Interest: The authors declare that there is no conflict of interest.

Nomenclature

E_a	Activation energy (kJ/mol)
A	Pre-exponential factor (min^{-1})
X	Conversion
TM	trademark
k	Rate constant of reaction
m_o	Initial mass of sample (mg)
m_t	Instantaneous mass of sample (mg)
$\overline{T}$	Absolute temperature (K)
T_m	Maximum peak temperature (°C)
β	Heating rate (°C/min)
R	Universal gas constant (kJ/mol.K)
T	Temperature (°C)
m_f	Final residual mass of sample (mg)
t	Time (min)

References

1. Kweku, D.W.; Bismark, O.; Maxwell, A.; Desmond, K.A.; Danso, K.B.; Oti-Mensah, E.A.; Quachie, A.T.; Adormaa, B.B.; Koomson, D. Greenhouse Effect: Greenhouse Gases and Their Impact on Global Warming. *J. Sci. Res. Rep.* **2018**, *17*, 1–9. [CrossRef]
2. Hassanpouryouzband, A.; Joonaki, E.; Edlmann, K.; Haszeldine, R.S. Offshore Geological Storage of Hydrogen: Is This Our Best Option to Achieve Net-Zero? *ACS Energy Lett.* **2021**, *6*, 2181–2186. [CrossRef]
3. Ahmad, T.; Zhang, D. A critical review of comparative global historical energy consumption and future demand: The story told so far. *Energy Rep.* **2020**, *6*, 1973–1991. [CrossRef]
4. Rahman, M.; Rahman, S.; Rahman, M.; Hasan, M.; Shoaib, S.; Rushd, S. Greenhouse Gas Emissions from Solid Waste Management in Saudi Arabia—Analysis of Growth Dynamics and Mitigation Opportunities. *Appl. Sci.* **2021**, *11*, 1737. [CrossRef]
5. De la Barrera, B.; Hooda, P. Greenhouse gas emissions of waste management processes and options: A case study. *Waste Manag. Res.* **2016**, *34*, 658–665. [CrossRef]
6. Klass, D.L. *Biomass for Renewable Energy, Fuels, and Chemicals*; Academic Press: San Diego, CA, USA, 1998.
7. Saidur, R.; Abdelaziz, E.; Demirbas, A.; Hossain, M.; Mekhilef, S. A review on biomass as a fuel for boilers. *Renew. Sustain. Energy Rev.* **2011**, *15*, 2262–2289. [CrossRef]
8. Adhikari, S.; Nam, H.; Chakraborty, J.P. Conversion of Solid Wastes to Fuels and Chemicals Through Pyrolysis. *Waste Biorefinery* **2018**, 239–263. [CrossRef]
9. Harjanne, A.; Korhonen, J. Abandoning the concept of renewable energy. *Energy Policy* **2019**, *127*, 330–340. [CrossRef]
10. Zafar, S. Municipal Solid Wastes in Qatar | Blogging Hub. 2019. Available online: https://www.cleantechloops.com/municipal-solid-waste-in-qatar/ (accessed on 20 October 2020).
11. Diaz-Barriga-Fernandez, A.; Santibañez-Aguilar, J.; González-Campos, J.; Nápoles-Rivera, F.; Ponce-Ortega, J.; El-Halwagi, M. Strategic planning for managing municipal solid wastes with consideration of multiple stakeholders. *Comput. Aided Chem. Eng. Elsevier.* **2018**, *44*, 1597–1602.
12. Alam, O.; Qiao, X. An in-depth review on municipal solid waste management, treatment and disposal in Bangla-desh. *Sustain. Cities Soc.* **2020**, *52*, 101775. [CrossRef]
13. Syguła, E.; Świechowski, K.; Hejna, M.; Kunaszyk, I.; Białowiec, A. Municipal Solid Waste Thermal Analysis—Pyrolysis Kinetics and Decomposition Reactions. *Energies* **2021**, *14*, 4510. [CrossRef]
14. Wang, Y.; Kinoshita, C. Kinetic model of biomass gasification. *Sol. Energy* **1993**, *51*, 19–25. [CrossRef]
15. Arshad, M.A.; Maaroufi, A.; Benavente, R.; Pinto, G. Kinetics of the Thermal Decomposition Mechanisms of Con-ducting and Non-conducting epoxy/Al Composites. *J. Mater. Environ. Sci* **2014**, *5*, 1342–1354.
16. Nakamura, S. Fundamentals of Chemical Reaction Kinetics. *Sol. Chem. Energy Convers. Theory Appl. Cham Springer Int. Publ.* **2016**. Available online: https://link.springer.com/chapter/10.1007/978-3-319-25400-5_4 (accessed on 12 May 2021).
17. Mamleev, V.; Bourbigot, S.; Le Bras, M.; Lefebvre, J. Three model-free methods for calculation of activation energy in TG. *J. Therm. Anal. Calorim.* **2004**, *78*, 1009–1027. [CrossRef]
18. Slopiecka, K.; Bartocci, P.; Fantozzi, F. Thermogravimetric analysis and kinetic study of poplar wood pyrolysis. *Appl. Energy* **2012**, *97*, 491–497. [CrossRef]
19. Benhacine, F.; Yahiaoui, F.; Hadj-Hamou, A. Thermal stability and kinetic study of isotactic polypropyl-ene/Algerian bentonite nanocomposites prepared via melt blending. *J. Polym.* **2014**, *2014*, 1–9. [CrossRef]
20. Cui, H.W.; Jiu, J.; Sugahara, T.; Nagao, S.; Suganuma, K.; Uchida, H.; Schroder, K. Using the Friedman method to study the thermal degradation kinetics of photonically cured electrical-ly conductive adhesives. *J. Therm. Anal. Calorim.* **2015**, *119*, 425–433. [CrossRef]
21. Nelson, J. Determination of Kinetic Parameters of Six Ablation Polymers by Thermogravimetric Analysis. 1967. Available online: https://apps.dtic.mil/sti/citations/ADA306600 (accessed on 12 May 2021).

22. Kessler, M.R.; White, S.R. Cure kinetics of the ring-opening metathesis polymerization of dicyclopentadiene. *J. Polym. Sci. Part A: Polym. Chem.* **2002**, *40*, 2373–2383. [CrossRef]
23. Li, A.; Gao, N.; Quan, C. Thermogravimetric analysis and kinetic study on large particles of printed circuit board wastes Furfural clean production View project MSW Gasification View project Thermogravimetric analysis and kinetic study on large particles of printed circuit board wastes. *Waste Manag.* **2009**, *29*, 2353–2360.
24. Morais, L.C.; Maia, A.A.D.; Guandique, M.E.G.; Rosa, A.H. *Pyrolysis and Combustion of Sugarcane Bagasse*; Springer: Berlin/Heidelberg, Germany, 2017; Volume 129, pp. 1813–1822.
25. Gerassimidou, S.; Velis, A.C.; Williams, P.T.; Komilis, D. Characterisation and composition identification of waste-derived fuels obtained from municipal solid waste using thermogravimetry: A review. *Waste Manag. Res.* **2020**, *38*, 942–965. [CrossRef]
26. Guida, M.Y.; Lanaya, S.; Rbihi, Z.; Hannioui, A. Thermal degradation behaviors of sawdust wood waste: Pyrolysis kinetic and mechanism. *J. Mater. Environ. Sci.* **2019**, *10*, 742–755.
27. Singh, S.; Wu, C.; Williams, P. Pyrolysis of waste materials using TGA-MS and TGA-FTIR as complementary characterisation techniques. *J. Anal. Appl. Pyrolysis* **2012**, *94*, 99–107. [CrossRef]
28. Chen, S.; Meng, A.; Long, Y.; Zhou, H.; Li, Q.; Zhang, Y. TGA pyrolysis and gasification of combustible municipal solid waste. *J. Energy Inst.* **2015**, *88*, 332–343. [CrossRef]
29. Azam, M.; Setoodeh Jahromy, S.; Raza, W.; Jordan, C.; Harasek, M.; Winter, F. Comparison of the combustion characteristics and kinetic study of coal, municipal solid waste, and refuse-derived fuel: Model-fitting methods. *Wiley Online Libr.* **2019**, *7*, 2646–2657. [CrossRef]
30. Szűcs, T.; Szentannai, P.; Szilágyi, I.M.; Bakos, L.P. Comparing different reaction models for combustion kinetics of solid recovered fuel. *J. Therm. Anal. Calorim.* **2019**, *139*, 555–565. [CrossRef]
31. Miskolczi, N.; Buyong, F. Thermogravimetric analysis and pyrolysis kinetic study of Malaysian refuse derived fuels Production of methane gas from biomass by using anaerobic digestion View project FACE Project UKM View pro-ject. *Taylor Fr.* **2010**, *83*, 125–132.
32. Liu, Z.; Jiang, Z.; Fei, B.; Liu, X.E. Thermal decomposition of Chinese fir. *BioResources* **2013**, *8*, 2013. [CrossRef]
33. Zan, R.; Wang, W.; Xu, R.; Schenk, J.; Zheng, H.; Wang, H. Gasification Characteristics and Kinetics of Unburned Pulverized Coal in Blast Furnaces. *Energies* **2019**, *12*, 4324. [CrossRef]
34. Jess, A.; Andresen, A.-K. Influence of mass transfer on thermogravimetric analysis of combustion and gasification reactivity of coke. *Fuel* **2010**, *89*, 1541–1548. [CrossRef]
35. Jayaraman, K.; Gokalp, I.; Bonifaci, E.; Merlo, N. Kinetics of steam and CO 2 gasification of high ash coal–char produced under various heating rates. *Fuel* **2015**, *154*, 370–379. [CrossRef]
36. Gu, X.; Zhou, X.; Wu, M.; Wang, X.; Chen, Y.; Cheng, K. Kinetic Study of Pine Sawdust Pyrolysis via TG/DTG Analysis. *Cellulose Chem. Technol.* **2017**, *51*, 387–394.
37. Nisar, J.; Khan, M.A.; Iqbal, M.; Shah, A.; Khan, R.A.; Sayed, M.; Mahmood, T. Comparative Study of Kinetics of the Thermal Decomposition of Polypropylene Using Different Methods. *Adv. Polym. Technol.* **2018**, *37*, 1168–1175. [CrossRef]
38. Chew, J.J.; Soh, M.; Sunarso, J.; Yong, S.-T.; Doshi, V.; Bhattacharya, S. Isothermal kinetic study of CO_2 gasification of torrefied oil palm biomass. *Biomass Bioenergy* **2020**, *134*, 105487. [CrossRef]
39. Muravyev, N.V.; Pivkina, A.N.; Koga, N. Critical Appraisal of Kinetic Calculation Methods Applied to Overlapping Multistep Reactions. *Molecules* **2019**, *24*, 2298. [CrossRef]
40. Wong, F.F.; Lin, C.M.; Chen, K.-L.; Shen, Y.-H.; Huang, J.-J. Improvement of the thermal latency for epoxy-phenolic resins by novel amphiphatic imidazole catalysts. *Macromol. Res.* **2010**, *18*, 324–330. [CrossRef]
41. Government Communications Office. Qatar National Vision 2030. *Fourth Pillar Environ. Dev.* **2020**, 209–230.